AD-765 692

AN EMPIRICAL EQUATION FOR PREDICTION OF A TRANSITION LOCATION ON CONES IN SUPER-OR HYPERSONIC FLIGHT

Neal Tetervin

Naval Ordnance Laboratory

Prepared for:

Naval Ordnance Systems Command

14 June 1973

NOLTR 73-127

AN EMPIRICAL EQUATION FOR PREDICTION OF TRANSITION LOCATION ON CONES IN SUPER- OR-HYPERSONIC FLIGHT

BY
Neal Tetervin

14 JUNE 1973

NOL
NAVAL ORDNANCE LABORATORY, WHITE OAK, SILVER SPRING, MARYLAND

NOLTR 73-127

UNCLASSIFIED

Security Classification

DOCUMENT CONTROL DATA - R & D

(Security classification of title, body of abstract and indexing annotation must be entered when the overall report is classified)

1. ORIGINATING ACTIVITY (Corporate author)
Naval Ordnance Laboratory
Silver Spring, Maryland 20910

2a. REPORT SECURITY CLASSIFICATION
Unclassified

2b. GROUP

3. REPORT TITLE
An Empirical Equation for Prediction of Transition Location on Cones in Supersonic or Hypersonic Flight

4. DESCRIPTIVE NOTES (Type of report and inclusive dates)

5. AUTHOR(S) (First name, middle initial, last name)
Neal Tetervin

6. REPORT DATE
14 June 1973

7a. TOTAL NO. OF PAGES
24

7b. NO. OF REFS
9

8a. CONTRACT OR GRANT NO

b. PROJECT NO ORD-35A-001/UF/32-322-505

c.

d.

9a. ORIGINATOR'S REPORT NUMBER(S)
NOLTR 73-127

9b. OTHER REPORT NO(S) (Any other numbers that may be assigned this report)

10. DISTRIBUTION STATEMENT
Approved for public release; distribution unlimited.

11. SUPPLEMENTARY NOTES

12. SPONSORING MILITARY ACTIVITY
Naval Ordnance Systems Command
Washington, D. C. 20360

13. ABSTRACT

An empirical equation has been developed for the prediction of transition location on blunt and sharp cones. The equation predicts the transition location fairly well for 48 ballistics range tests for cones without ablation and for 40 flight tests for cones with ablation ranging from zero to large. The equation is applicable for cones in supersonic or hypersonic flight. The experimental data cover a range of local Mach numbers at transition from 2.8 to 14.7 and a range of the ratio of local wall to local stream temperature at transition from .074 to 1.43.

DD FORM 1 NOV 68 1473 (PAGE 1)

S/N 0101-807-6801

Unclassified

Security Classification

14 KEY WORDS	LINK A		LINK B		LINK C	
	ROLE	WT	ROLE	WT	ROLE	WT
Transition Cones Re-entry bodies Supersonic flight Hypersonic flight						

AN EMPIRICAL EQUATION FOR PREDICTION OF TRANSITION LOCATION ON CONES IN SUPER- OR HYPERSONIC FLIGHT

Prepared by
Neal Tetervin

ABSTRACT: An empirical equation has been developed for the prediction of transition location on blunt and sharp cones. The equation predicts the transition location fairly well for 48 ballistics range tests for cones without ablation and for 40 flight tests for cones with ablation ranging from zero to large. The equation is applicable for cones in supersonic or hypersonic flight. The experimental data cover a range of local Mach numbers at transition from 2.8 to 14.7 and a range of the ratio of local wall to local stream temperature at transition from .074 to 1.43.

NAVAL ORDNANCE LABORATORY
Silver Spring, Maryland

NOLTR 73-127 14 June 1973

AN EMPIRICAL EQUATION FOR PREDICTION OF TRANSITION LOCATION ON CONES IN SUPER-OR HYPERSONIC FLIGHT

This report presents the development of an empirical equation for the prediction of the location of transition on cones in supersonic or hypersonic flight. This work was supported by the Naval Ordnance Systems Command under Task No. ORD 35A-001/UF/32-322-505.

Appreciation is expressed to A. Martellucci of General Electric Company who made available a preliminary copy of Reference 9.

ROBERT WILLIAMSON II
Captain, USN

L. H. Schindel

L. H. SCHINDEL
By direction

CONTENTS

ILLUSTRATIONS

TABLES

Symbols

a	constant
A_{CT}	area of cone cross section at X_T
C_o	constant
C_1	constant
C_f	$\frac{\tau_w}{\frac{\rho_e u_e^2}{2}}$ friction coefficient
D	$\mu \overline{\left(\frac{\partial u'}{\partial y}\right)^2}$, approximation to the rate of dissipation of fluctuation kinetic energy per unit volume
G	transition parameter, defined by Equation (34)
G_*	transition parameter, defined by Equation (33)
k	constant
K	constant
M	Mach number
m	constant
$\overline{\dot{m}_f}$	$\frac{\int_{nose}^{X_T} \rho_w v_w dS}{\rho_\infty U_\infty A_{CT}}$ normalized mass ratio for frustum, (same as $\dot{m}$ of Table 7, Reference 9)
p	constant
P	$-\rho\overline{u'v'}\ \frac{\partial u}{\partial y}$, approximation to the rate of production of fluctuation kinetic energy per unit volume
P_r	Prandtl number
$\overline{q^2}$	$\overline{(u'^2 + v'^2 + w'^2)}$, twice the fluctuation kinetic energy per unit mass
r	recovery factor
R_{e_θ}	$\frac{\rho_e u_e \theta}{\mu_e}$, Reynolds number based on momentum thickness θ
R_{e_X}	$\frac{\rho_e u_e X}{\mu_e}$, Reynolds number based on X
S	surface area
T	temperature

Symbols

u	X component of velocity
U_∞	free stream velocity, far ahead of body
v	y component of velocity
X	distance along surface of cone in plane through axis of symmetry
y	distance perpendicular to surface
γ	ratio of specific heats
θ	$\int_0^\infty \frac{\rho u}{\rho_e u_e} \left(1 - \frac{u}{u_e}\right) dy$ momentum thickness
μ	viscosity
ν	kinematic viscosity
ρ	density
τ	shear stress

Subscripts

e	at outer edge of boundary layer
i	at value of X at which laminar boundary layer first becomes unstable
r	recovery value
T	at transition
w	at surface
$*$	at reference conditions
∞	far ahead of body

Superscripts

$\overline{(\ )}$	time average value
$(\ )'$	fluctuating quantity

INTRODUCTION

The object of this investigation is to develop a method for predicting the location of transition from laminar to turbulent boundary-layer flow on conical re-entry bodies. Accurate prediction of the transition location is important because the heat flow to a surface is much larger when the boundary layer on the surface is turbulent than when it is laminar. Because of the high heat-transfer rates during re-entry, the difference between turbulent and laminar heat-transfer rates is so large that the variation of transition location with altitude is an important factor in the choice of surface material and its thickness distribution over the body. Material that is too thick may fail because of thermal strain. Material that is too thin may fail by burning through. Moreover, the nose shape for an ablating body depends on the variation of the transition location with altitude and thus so do the aerodynamic characteristics of the body.

Attempts to predict transition location began about forty years ago and pertained to wings and bodies. The main parameter was usually a quantity at the transition point, ordinarily a boundary layer-thickness Reynolds number. The assumption that transition occurs at a constant value of a boundary-layer Reynolds number sometimes gave usable results for a more-or-less fixed pressure distribution. Later, Michel (Ref. (1)) developed a more general and seemingly more reliable empirical relation between $R_{e\theta}$ and R_{e_x} at transition on airfoils. This correlation is claimed to give sufficiently accurate calculated profile drag coefficients (Ref. (2)). More complicated methods have also been tried. One is a correlation of $(R_{e\theta_T} - R_{e\theta_i})$ with the average value of the velocity profile shape parameter between X_T and X_i (Ref. (3)). Another (Ref. (4)) uses a family of similar profiles to represent the velocity profiles in a laminar boundary layer. For each of the similar profiles the amplification rate of a small oscillation in the velocity in the laminar boundary layer is computed as a function of the Reynolds number. The amplification rates for the velocity profiles along the boundary layer are used to calculate the total amplification of a small disturbance that begins at the stagnation point and moves downstream. The total amplification up to the measured transition point was calculated for a number of cases. Transition usually occurred for an amplification of between about e^7 and e^{12}. A value of about e^{10} seemed to give a good correlation between the measured and calculated values of $R_{e_{x_T}}$. This method is complicated and seems not to be used by Smith, its developer. In Smith's latest paper (Ref. (2)) he uses Michel's method. Thus, about forty years after the first attempts, the preferred method for the prediction of transition in incompressible flow seems to be Michel's method, an empirical relation between $R_{e\theta_T}$ and $R_{e_{x_T}}$, whose limits of applicability are indefinite. Moreover, Michel's relation (Ref. (2)) has not been shown to apply when there is flow through the surface or when the surface is rough.

For compressible flow it is more difficult to predict the transition location than it is for incompressible flow. For incompressible flow over smooth solid surfaces only the pressure distribution and the Reynolds number matter. For compressible flow there are also the Mach number and the wall-to-stream temperature ratio. In practical problems, flow through the surface and roughness are additional parameters.

As already mentioned, the object of the present investigation is to develop a method for predicting the transition location on conical re-entry bodies. The method consists of attempting to find variables that allow a correlation between them and the transition location. Only flight and ballistics-range data are used in order to avoid the transition-causing-disturbances emitted from wind-tunnel wall turbulent boundary layers. Although some sound disturbances can be present in a ballistics range, the inference from Reference 5 is that such disturbances probably have even less effect on transition than those in a wind tunnel whose walls are covered by laminar layers.

ANALYSIS

A suggestion for choosing correlation parameters is sought from the velocity fluctuation kinetic energy equation (Ref. (6)). An approximation to the production of fluctuation energy is taken as $-\rho\overline{u'v'}\,\frac{\partial u}{\partial y}$ and an approximation to its dissipation as $\mu\overline{(\frac{\partial u'}{\partial y})^2}$. The ratio $\frac{P}{D}$ between production and dissipation of fluctuation energy is thus

$$\frac{P}{D} \sim \frac{-\rho\overline{u'v'}\,\frac{\partial u}{\partial y}}{\mu\overline{(\frac{\partial u'}{\partial y})^2}} \tag{1}$$

To put $\frac{P}{D}$ in a more useable form the terms in Equation (1) are written in non-dimensional form so that Equation (1) becomes

$$\frac{P}{D} \sim R_{e_\theta}\,(\frac{\nu_e}{\nu})\,\frac{\left(\frac{u}{u_e}\right)\left(\frac{\overline{u'v'}}{u_e^2}\right)}{\overline{\left(\frac{\partial \frac{u'}{u_e}}{\partial y/\theta}\right)^2}} \tag{2}$$

The term $\left(\frac{\partial \frac{u}{ue}}{\partial y/\theta}\right)$ is assumed to be proportional to $\left(\frac{\partial u/ue}{\partial y/\theta}\right)_w$ which can be written ,

$$\left(\frac{\partial \frac{u}{ue}}{\partial \frac{y}{\theta}}\right)_w = \frac{C_f}{2} R_{e_\theta} \frac{\mu e}{\mu w} \tag{3}$$

Then Equation (2) becomes

$$\frac{P}{D} \sim R_{e_\theta}{}^2 \left(\frac{\nu e}{\nu}\right) \left(\frac{\mu e}{\mu w}\right) \frac{C_f}{2} \frac{\left(\frac{\overline{u'v'}}{ue^2}\right)}{\left(\frac{\partial \frac{u'}{ue}}{\partial y/\theta}\right)^2} \tag{4}$$

It is now assumed that both $\frac{\overline{u'v'}}{ue^2}$ and $\left(\frac{\partial \frac{u'}{ue}}{\partial \frac{y}{\theta}}\right)^2$ are proportional to the maximum value of $\overline{\left(\frac{u'}{ue}\right)^2}$ at a cross section of the boundary layer and thus to one another. Then Equation (4) becomes

$$\frac{P}{D} \sim R_{e_\theta}{}^2 \left(\frac{\nu e}{\nu}\right) \left(\frac{\mu e}{\mu w}\right) \frac{C_f}{2} \tag{5}$$

The friction coefficient in Equation (5) is approximated by the reference temperature formula for a laminar boundary layer (Ref. (7)),

$$\frac{C_f}{2} = \frac{k}{R_{e_\theta}} \left(\frac{\mu *}{\mu e}\right) \left(\frac{\rho *}{\rho e}\right) \tag{6}$$

The quantity ν in Equation (5) is evaluated at the reference temperature. Then Equation (5, becomes

$$\frac{P}{D} \sim R_{e_\theta} \left(\frac{\mu e}{\mu w}\right) \left(\frac{\rho *}{\rho e}\right)^2 \tag{7}$$

The viscosity is assumed to be given with sufficient accuracy by

$$\frac{\mu e}{\mu w} = \left(\frac{Te}{Tw}\right)^m \tag{8}$$

Then Equation (7) becomes

$$\frac{P}{D} \sim R_{e_\theta} \left(\frac{Te}{Tw}\right)^m \left(\frac{Te}{T*}\right)^2 \tag{9}$$

The equation for the rate of change of fluctuation energy is approximated by

$$\rho_e u_e \frac{\partial \overline{q^2}}{\partial X} \sim -\rho \overline{u'v'} \frac{\partial u}{\partial y} - \mu \overline{\left(\frac{\partial u'}{\partial y}\right)^2} \tag{10}$$

or with Equation (1)

$$\rho_e u_e \frac{\partial \overline{q^2}}{\partial X} \sim \mu \overline{\left(\frac{\partial u'}{\partial y}\right)^2} \left[\frac{P}{D} - 1\right] \tag{11}$$

When the variation of u_e with X is neglected, Equation (11) can be written as

$$\frac{\partial \frac{\overline{q^2}}{u_e^2}}{\partial X} \sim \frac{\left(\frac{\mu}{\mu_e}\right)}{\theta \, Re_\theta} \overline{\left(\frac{\partial u'/u_e}{\partial \frac{Y}{\theta}}\right)^2} \left[\frac{P}{D} - 1\right] \tag{12}$$

The ratio $\left(\frac{\mu}{\mu_e}\right)$ in Equation (12) is replaced by $\left(\frac{\mu^*}{\mu_e}\right)$ and Equation (9) is used for $\frac{P}{D}$. Then Equation (12) becomes

$$\frac{\partial \frac{\overline{q^2}}{u_e^2}}{\partial X} \sim \frac{\left(\frac{\mu^*}{\mu_e}\right)}{\theta \, Re_\theta} \overline{\left(\frac{\partial \frac{u'}{u_e}}{\partial \frac{Y}{\theta}}\right)^2} \left[Re_\theta \left(\frac{Te}{Tw}\right)^m \left(\frac{Te}{Tw}\right)^2 - 1\right] \tag{13}$$

or

$$\frac{\partial \frac{\overline{q^2}}{u_e^2}}{\partial X} \sim \frac{\left(\frac{\mu^*}{\mu_e}\right)}{\theta} \overline{\left(\frac{\partial \frac{u'}{u_e}}{\partial \frac{Y}{\theta}}\right)^2} \left[\left(\frac{Te}{Tw}\right)^m \left(\frac{Te}{T^*}\right)^2 - \frac{1}{Re_\theta}\right] \tag{14}$$

It is assumed that $\frac{1}{Re_\theta}$ is negligible when compared with $\left(\frac{Te}{Tw}\right)^m \left(\frac{Te}{T^*}\right)^2$; Equation (14) then becomes

$$\frac{\partial \frac{\overline{q^2}}{u_e^2}}{\partial X} \sim \frac{\left(\frac{Te}{Tw}\right)^m \left(\frac{Te}{T^*}\right)^{2-m}}{\theta} \overline{\left(\frac{\partial \frac{u'}{u_e}}{\partial Y/\theta}\right)^2} \tag{15}$$

The term $\overline{\left(\frac{\partial \frac{u'}{ue}}{\partial y/\theta}\right)^2}$ is assumed to be proportional to the magnitude of the fluctuations in velocity and thus to $(\overline{\frac{q^2}{ue^2}})$. Then Equation (15) becomes

$$\frac{1}{(\overline{\frac{q^2}{ue^2}})} \quad \frac{\partial \overline{\frac{q^2}{ue^2}}}{\partial X} \sim \frac{(\frac{Te}{Tw})^m \quad (\frac{Te}{T*})^{2-m}}{\theta} \tag{16}$$

or

$$\Delta \ (\overline{\frac{q^2}{ue^2}}) \sim \exp\left(\int \frac{dX}{(\frac{Tw}{Te})^m \ (\frac{T*}{Te})^{2-m}_{\theta}}\right) \tag{17}$$

If $\Delta(\overline{\frac{q^2}{ue^2}})$ has to reach some more-or-less fixed value for transition to occur, Equation (17) implies that

$$\int \frac{dX}{(\frac{Tw}{Te})^m \ (\frac{T*}{Te})^{2-m}_{\theta}} = K \tag{18}$$

For the purpose of this rough analysis the ratio $\frac{dX}{\theta}$ in Equation (18) is replaced by $\frac{dR_{e_X}}{R_{e_\theta}}$; this neglects the variation with X of the local Reynolds number per foot, $\frac{ue}{\nu e}$. Then Equation (18) becomes

$$\int_{R_{e_{X_T}}} \frac{dR_{e_X}}{(\frac{Tw}{Te})^m \ (\frac{T*}{Te})^{2-m} \ R_{e_\theta}} = K \tag{19}$$

For cases in which the integrand in Equation (19) varies with R_{e_X} in roughly the same manner, the quantity $[(\frac{Tw}{Te})^m \ (\frac{T*}{Te})^{2-m} R_{e_\theta}]_T$ should fall in a more or less narrow band when plotted against $R_{e_{X_T}}$. That is, approximately,

$$Re_{x_T} = F\left[\left(\frac{Tw}{Te}\right)^{m}\left(\frac{T^*}{Te}\right)^{2-m} Re_\theta\right]_T \tag{20}$$

The value 2/3 for m in Equation (20) is assumed to be precise enough for the present analysis. Also, the expression for $\left(\frac{T^*}{Te}\right)$ in Equation (20) is taken from Reference (7) and is

$$\frac{T^*}{Te} = \frac{1}{2}\left(\frac{Tw}{Te} + 1\right) + .22r\,\frac{\gamma-1}{2}\,Me^2 \tag{21}$$

For the present correlation attempt, the recovery factor r in Equation (21) is taken as .84 and γ is taken as 1.4. Equation (21) then becomes

$$\frac{T^*}{Te} = \frac{1}{2}\left(\frac{Tw}{Te} + 1\right) + .037\ Me^2 \tag{22}$$

The result then is

$$Re_{x_T} = F\left\{\left(\frac{Tw}{Te}\right)^{2/3}\left[\frac{1}{2}\left(\frac{Tw}{Te} + 1\right) + .037\ Me^2\right]^{4/3} Re_\theta\right\}_T \tag{23}$$

The data used to test the supposition (Eq. (23)) are those in References (8) and (9). The data from Reference (8) are for no ablation. There are three tables of data in Reference (8). The tables give the values of Re_{x_T}, Re_{θ_T}, and Me_T which were used in Equation (23). The values of $\left(\frac{Tw}{Te}\right)_T$ needed in Equation (23) were obtained from the values of $\left(\frac{Tw}{Tr}\right)_T$ given in the tables of Reference (8) by the expression

$$\frac{Tw}{Te} = \frac{Tw}{Tr}\left(1+\sqrt{Pr}\,\frac{\gamma-1}{2}\,Me^2\right), \tag{24}$$

or with $\sqrt{Pr} = .84$ and $\gamma = 1.4$,

$$\frac{Tw}{Te} = \frac{Tw}{Tr}\left(1+.168\ Me^2\right) \tag{25}$$

The first table in Reference (8) is headed, "Temperature ratio investigations." This table contains data for sharp 5-degree half-angle cones tested through a free-stream Mach range from 2.95 to 8.29. The second table is headed, "Mach number and body geometry investigations." This table contains data for 3, 5, 6.3, and 9-degree

half-angle cones with nose-to-base radius ratios from .012 to .10. The free-stream Mach numbers varied from 6.7 to 12.8. The third table is headed, "Drag Method." This table contains data for 6.3- and 9-degree half-angle cones with nose-to-base radius ratios from .017 to .12. The free-stream Mach numbers ranged from 9 to 15. The range in $\frac{T_w}{T_r}$ covered by the complete set of tests listed in the three tables was from .026 to .265.

The parameter $\left\{\left(\frac{T_w}{T_e}\right)^{2/3}\left[\frac{1}{2}\left(\frac{T_w}{T_e}+1\right)+.037M_e^2\right]^{4/3} Re_\theta\right\}_T$, called G_T, is plotted against Re_{x_T} in Figure 1(a); each set of data has its own symbol (see Table 1). The data lie in a fairly narrow band. The variation in Re_{x_T} for the same G_T is in general no larger than the variation in Re_{x_T} in Reference (8) for the same flight conditions.

The data shown in Figure 1(a) were fitted by a least-squares equation of the type

$$Re_{x_T} = a\, G_T^{\,p} \tag{26}$$

with the result

$$Re_{x_T} = 2.259 \times 10^4\, G_T^{\,.7764} \tag{27}$$

The plot of this equation is shown in Figure 1(b). The Equation (27) is plotted on a separate figure from Figure 1(a) so that the distribution of data in Figure 1(a) can be observed without the intrusion of the effect of a curve through the data. The dashed portion of the curve in Figure 1(b) is an extrapolation beyond the range of the data. The Equation (27) seems to fit the data with acceptable closeness. A better representation can probably be obtained by using a more complicated expression than Equation (26) or even by drawing in a curve by "eye."

In Figure 2(a) the 40 points of "high-quality" flight data from Reference (9) are shown. The identification code for each point in Figure 2(a) is given in Table II. The data cover a range of free-stream Mach number at transition from 3.17 to 23.70. The data include a range of cone angle, nose radius, and various combinations of materials for the nose and frustum of the cones. Specific information is given in a classified appendix to Reference (9).

When the points G_T, Re_{x_T} were first plotted, those for large values of $\dot{m}_f$, the ablation on the frustum of the cones, fell too far from those with small $\dot{m}_f$ for the present method of correlation to be satisfactory. The quantity $\dot{m}_f$ is called $\dot{m}$ in Table 7

of Reference (9). It was found that a satisfactory correlation for all the 40 points of Reference (9), both those for high and low ablation, was obtained when G_T was replaced by G^*_T where

$$G^*_T = G_T \quad \text{for } \bar{\dot{m}}_f \leq 10^{-3}$$

and

$$G^*_T = \frac{G_T}{\bar{\dot{m}}_f} \times 10^{-3} \quad \text{for } \bar{\dot{m}}_f \geq 10^{-3}.$$

The correlation shown in Figure 2(a) is G^*_T against Re_{x_T}. The values of $\bar{\dot{m}}_f$ are those given in Table 7 of Reference (9). The values of $\left(\frac{T_w}{T_e}\right)_T$ needed in Equation (23) were obtained from the values of $\left(\frac{T_w}{T_\infty}\right)_T$ given in Table 7 of Reference (9) by the relation

$$\frac{T_w}{T_e} = \frac{T_w}{T_\infty} \frac{1 + \frac{\gamma-1}{2} M_e^2}{1 + \frac{\gamma-1}{2} M_\infty^2} \tag{28}$$

or, for $\gamma = 1.4$,

$$\frac{T_w}{T_e} = \frac{T_w}{T_\infty} \frac{5 + M_e^2}{5 + M_\infty^2} \tag{29}$$

A least-squares expression that fits the data of Figure 2(a) in a satisfactory manner is

$$Re_{x_T} = 3.120 \times 10^4 \, G^*_T{}^{.7274} \tag{30}$$

A plot of this expression is shown in Figure 2(b).

Figure 3(a) shows all the data, both ballistics range and flight. A least-squares expression that gives a satisfactory fit for all the data in Figure 3(a) is

$$Re_{x_T} = 2.932 \times 10^4 \, G^*_T{}^{.7370} \tag{31}$$

A plot of this expression is shown in Figure 3(b).

Finally, summing up, the expression which correlates all the data considered is,

$$Re_{xT} = 2.932 \times 10^{4}\ G_{*T}^{.7370} \tag{32}$$

where

$$\left.\begin{aligned} G_{*} &= G \qquad \text{for } \bar{\dot{m}}_f \le 10^{-3} \\ \text{and} \quad G_{*} &= \frac{G}{\bar{\dot{m}}_f} \times 10^{-3} \quad \text{for } \bar{\dot{m}}_f \ge 10^{-3} \end{aligned}\right\} \tag{33}$$

and

$$G = \left(\frac{Tw}{Te}\right)^{2/3} \left[\frac{1}{2}\left(\frac{Tw}{Te} + 1\right) + .037\ Me^{2}\right]^{\frac{4}{3}} Re_{\theta} \tag{34}$$

The data correlated by Equation (32) cover a range of Me_T from 2.8 to 14.7, a range of $\left(\frac{Tw}{Te}\right)_T$ from .074 to 1.43, and a range of ablation parameter $\bar{\dot{m}}_f$ from 0 to 17.7×10^{-3}.

DISCUSSION

It is obvious from the derivation of the relation

$$Re_{xT} = F(G_{*T}) \tag{35}$$

that many approximations have been made. Consequently, although a satisfactory correlation has been obtained for the 88 points in Figure 3(a), there is no guarantee that experiments in which some conditions differ sufficiently from those for these 88 points will yield values of G_{*T} and Re_{xT} that will conform to the present correlation. One point that must be stressed is that Re_x, $\frac{Tw}{Te}$, Me, and Re_θ must be calculated by the same procedures used in References (8) and (9). The calculation procedures, especially for blunt cones and for cones whose shapes are changing because of ablation, are part of the correlation procedure. If other calculation methods are used, the user must be prepared to obtain new correlations, hopefully involving the same variables used in the present investigation.

In Michel's method (Refs. (1) and (2)) the computed curve of Re_θ versus Re_x intersects the correlation curve of $Re_{\theta T}$ versus Re_{xT} at a small angle. This often makes it difficult to obtain a definite value for $Re_{\theta T}$ or Re_{xT}. A trial of the present procedure was made for shot number 5885 and shot number 5874 (Table I), cones for which

T_e and M_e varied with X. For each of these two cones the intersection angle between the curve of G against Re_x and the correlation curve of Figure 3 was large enough so that Re_{x_T} could be read without difficulty. This is probably a general result for the present method. Thus, for $\frac{T_w}{T_e}$ and M_e independent of X, Equation (32) becomes

$$Re_{x_T} = Co\ Re_{\theta_T}^{.7370} \tag{36}$$

For a sharp cone, however,

$$Re_x = C_1\ Re_\theta^2 \tag{37}$$

The difference in the value of the exponent of Re_θ in Equations (36) and (37) probably implies an angle of intersection large enough to eliminate difficulty from this source.

The roughness of the surface does not appear as a parameter in the expression for G* even though transition is known to be affected by roughness. Because a correlation of the 88 points is obtained without a roughness parameter it probably means that the roughnesses of the various materials were small enough not to exert a noticeable effect.

Like the roughness, the blowing or ablation parameter $\frac{\rho_w v_w}{\rho_e u_e}$ does not appear explicitly in G*. The calculated Reynolds number Re_θ, however, depends on $\frac{\rho_w v_w}{\rho_e u_e}$ and so G* does depend on $\frac{\rho_w v_w}{\rho_e u_e}$.

Equation (20) was obtained from Equation (19) by limiting the cases to those for which the integrand in Equation (19) has roughly the same type of variation with Re_x. All of the data in References (8) and (9) seem to be for transition on the cone frustum. Consequently, if transition occurs on a blunt nose the variation of the integrand in Equation (19), which is G^{-1}, with Re_x may differ sufficiently from its variation on the frustum for a point G^*_T, Re_{x_T} to fall too far from the band of points in Figure 3. Experiments in which transition occurs naturally on smooth blunt noses are therefore desirable to test the correlation method's ability to predict transition on blunt noses. Some modification of the correlation may be necessary.

CONCLUSION

An empirical equation,

$$Re_{x_T} = 2.932 \times 10^4\ G^*_T{}^{.7370},$$

has been developed which predicts the transition location fairly well for 48 ballistics range tests for cones without ablation and for

40 flight tests for cones with ablation ranging from zero to large. The experimental data cover a range of M_{e_T} from 2.8 to 14.7, a range of $\left(\frac{Tw}{Te}\right)_T$ from .074 to 1.43, and a range of abiation parameter $\bar{\dot{m}}_f$ from 0 to 17.7 x 10^{-3}. Nose tips range from sharp to fairly blunt.

REFERENCES

1. Michel, R., "Determination du Point de Transition et Calcul de la Trainée des Profiles D'Ailes en Incompressible," Publication No. 58 O.N.E.R.A., 1952

2. Cebeci, T., Mosinskis, G. J., Smith, A.M.O., "Calculation of Viscous Drag in Incompressible Flows," Journal of Aircraft, Vol. 9, No. 10, Oct 1972, p 691

3. Granville, P. S., "The Calculation of the Viscous Drag of Bodies of Revolution," Report 849, Jul 1953, The David W. Taylor Model Basin

4. Jaffe, N. A., Okamura, T. T., Smith, A. M. O., "Determination of Spatial Amplification Factors and Their Application to Predicting Transition," AIAA Journal, Vol. 8, No. 2, Feb 1970, p 301

5. Potter, J. L., "Observations on the Influence of Ambient Pressure on Boundary-Layer Transition," AIAA Journal, Vol. 6, No. 10, Oct 1968, p 1907

6. Shamroth, S. J., McDonald, H., "Assessment of a Transitional Boundary Layer Theory at Low Hypersonic Mach numbers," NASA CR - 2131, Nov 1972

7. Eckert, E. R. G., "Survey on Heat Transfer at High Speeds," Aero. Res. Lab., WADC Tech. Rep. 54-70 (Contract AF 33(616)-2214), 1954

8. Sheetz, N. W., Jr., "Ballistics Range Boundary Layer Transition Measurements on Cones at Hypersonic Speeds," Viscous Drag Reduction, Ed. C. S. Wells, Plenum Press N.Y., 1969, p 53

9. Martellucci, A., Maguire, B. L., Neff, R. S., "Analysis of Flight Test Transition and Turbulent Heating Data, Part I - Boundary Layer Transition Results," NASA CR 129045, Nov 1972

TABLE I - IDENTIFICATION OF BALLISTICS RANGE DATA POINTS

Temperature Ratio Investigation X

Shot No.	$Re_{x_T} \times 10^{-6}$	Shot No.	$Re_{x_T} \times 10^{-6}$
4046	[illegible]	5041	5.25
4047	[illegible]	5042	4.40
4048	[illegible]	5043	9.20
4051	2.35	5049	7.67
4056	6.68	5050	5.36
4057	6.04	5467	4.98
4058	5.81	5468	4.42
4059	3.96	5469	4.91
4060	3.13	5470	4.69
5036	5.46	5462	9.32
5037	5.25	5474	11.56
5039	9.23	5475	7.29
5040	8.11		

Mach Number and Geometry Investigation +

5697	8.7	5840	1.3
5699	14.2	5843	11.1
5707	11.4	5857	12.6
5708	6.0	5874	0.5
5776	0.6	5881	5.3
5779	7.0	5885	15.2
5802	12.1	5895	1.9
5836	1.1		

Drag Method □

D1	6.8	D5	2.4
D2	6.8	D6	1.0
D3	16.3	D7	3.4
D4	5.6	D8	3.3

See Reference (8) for more information for each data point.

Data points that do not appear in Figures 1 or 3 have values of $G_T < 100$.

TABLE II - IDENTIFICATION OF FLIGHT DATA POINTS

Body	Symbol	$Re_{xT} \times 10^{-6}$	Body	Symbol	$Re_{xT} \times 10^{-6}$
B01	○	49.4	C05	▽	12.3
B02	○	29.1	C06	◇	4.35
B03	○	21.3	S01	◇	51.8
B04	○	18.8	S02	◇	86.5
B05	○	15.6	S03	◇	47.4
B06	○	7.17	S04	◇	34.6
B07	○	10.3	S05	▽	4.78
B08	○	1.45	S07	✧	9.50
B10	○	0.81	S08	⬡	17.0
B13	○	2.53	S09	⬡	1.18
B15	○	2.36	S10	⬡	29.1
B09	⌑	13.7	T01	◊	11.1
B11	◇	0.40	T02	◊	41.1
B12	◇	0.33	T03	◊	16.5
B14	◇	0.44	T05	◊	14.6
B16	◇	0.47	T06	◊	16.1
C01	▽	5.3	T07	◊	15.8
C02	◁	21.4	T08	◊	15.3
C03	◁	9.18	T04	▽	24.1
C04	◁	6.32	T10	▽	12.5

See Reference (9) for more information for each data point.

Data points that do not appear in Figures 2 or 3 have values of $G^*_T < 100$.

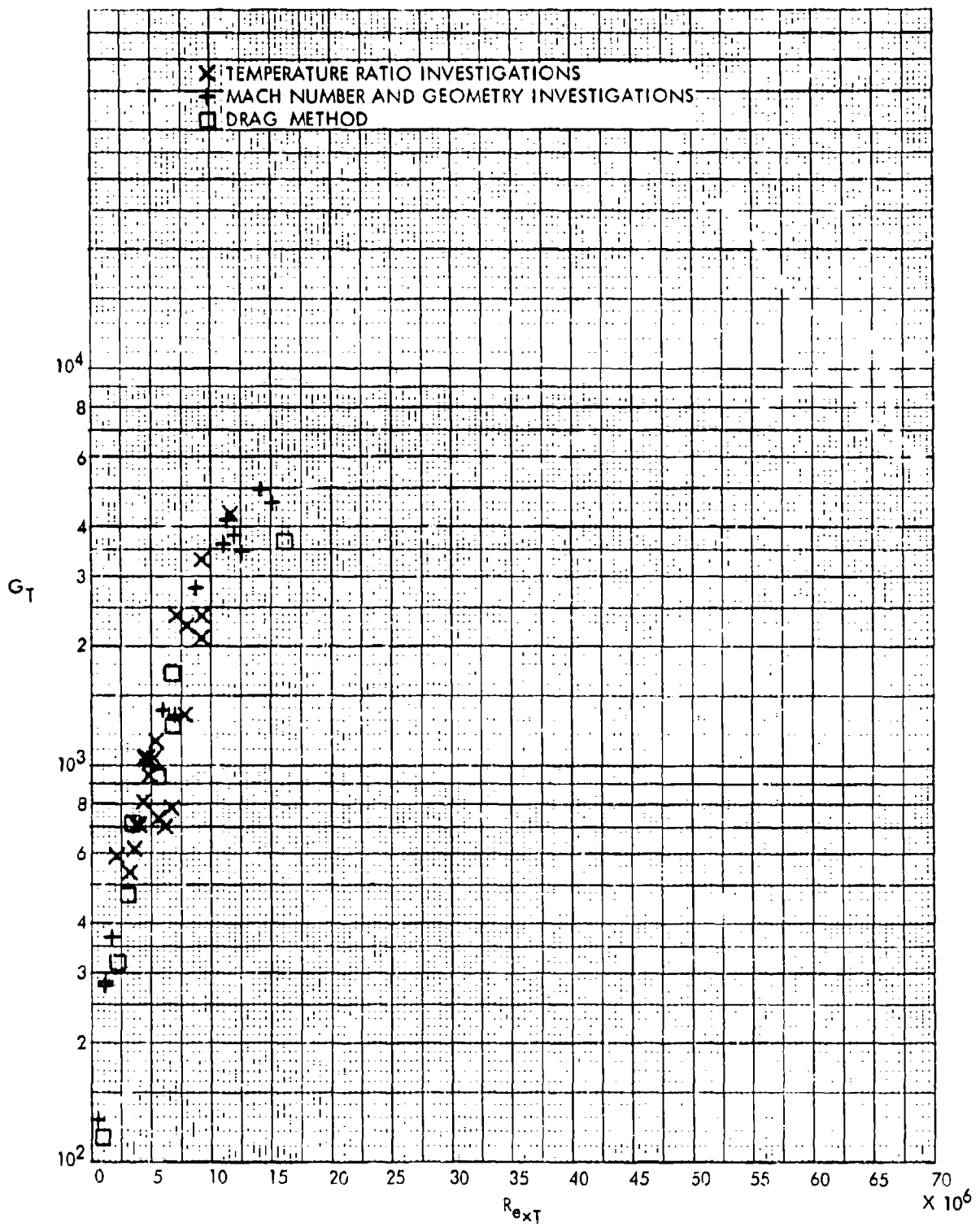

FIG. 1 (a) VARIATION OF TRANSITION PARAMETER G_T WITH TRANSITION REYNOLDS NUMBER $R_{e_{xT}}$ FOR BALLISTICS RANGE DATA, EXPERIMENTAL DATA (See Table I)

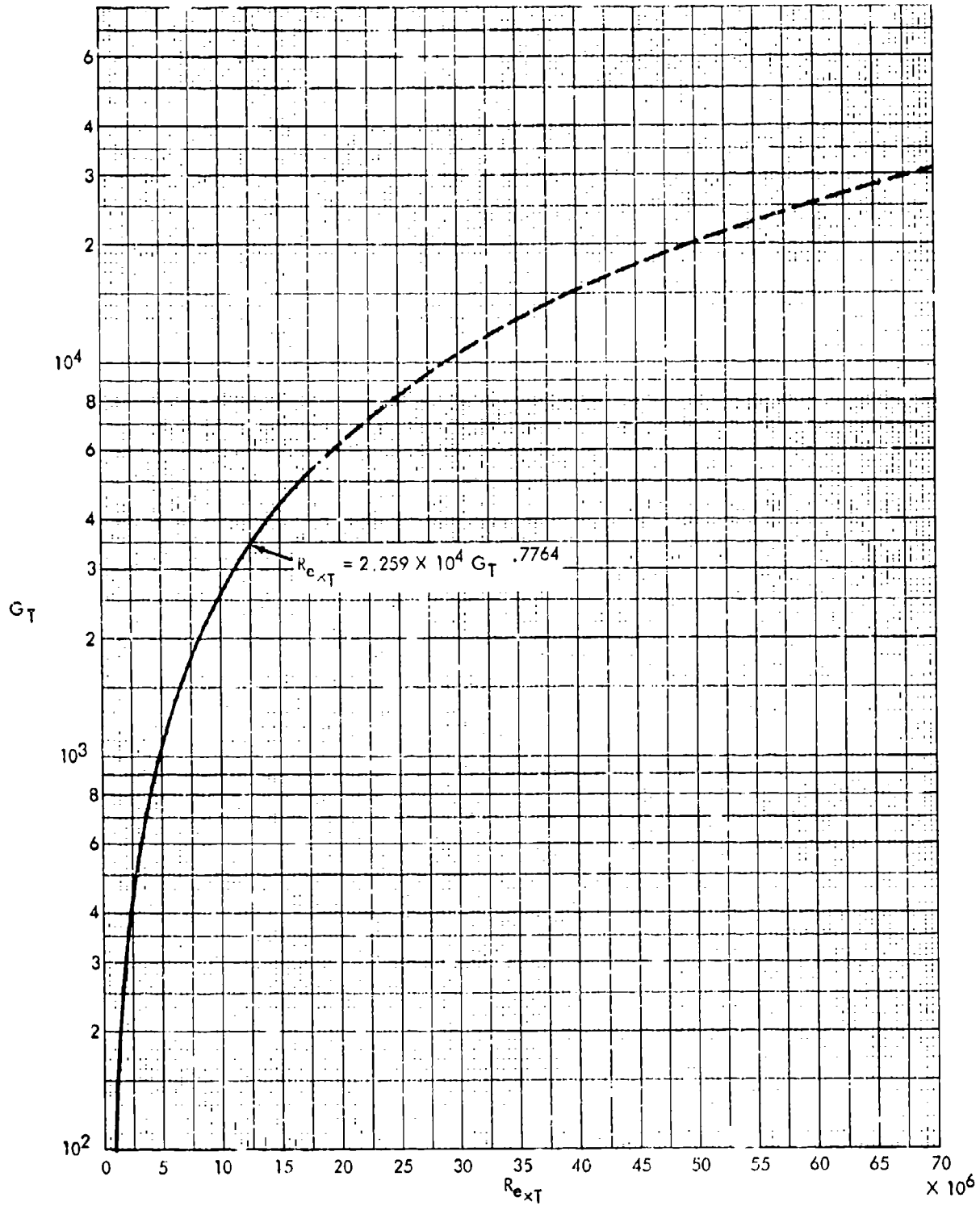

FIG. 1 (b) VARIATION OF TRANSITION PARAMETER G_T WITH TRANSITION REYNOLDS NUMBER $R_{e_{xT}}$ FOR BALLISTICS RANGE DATA, LEAST SQUARES EQUATION FOR EXPERIMENTAL DATA.

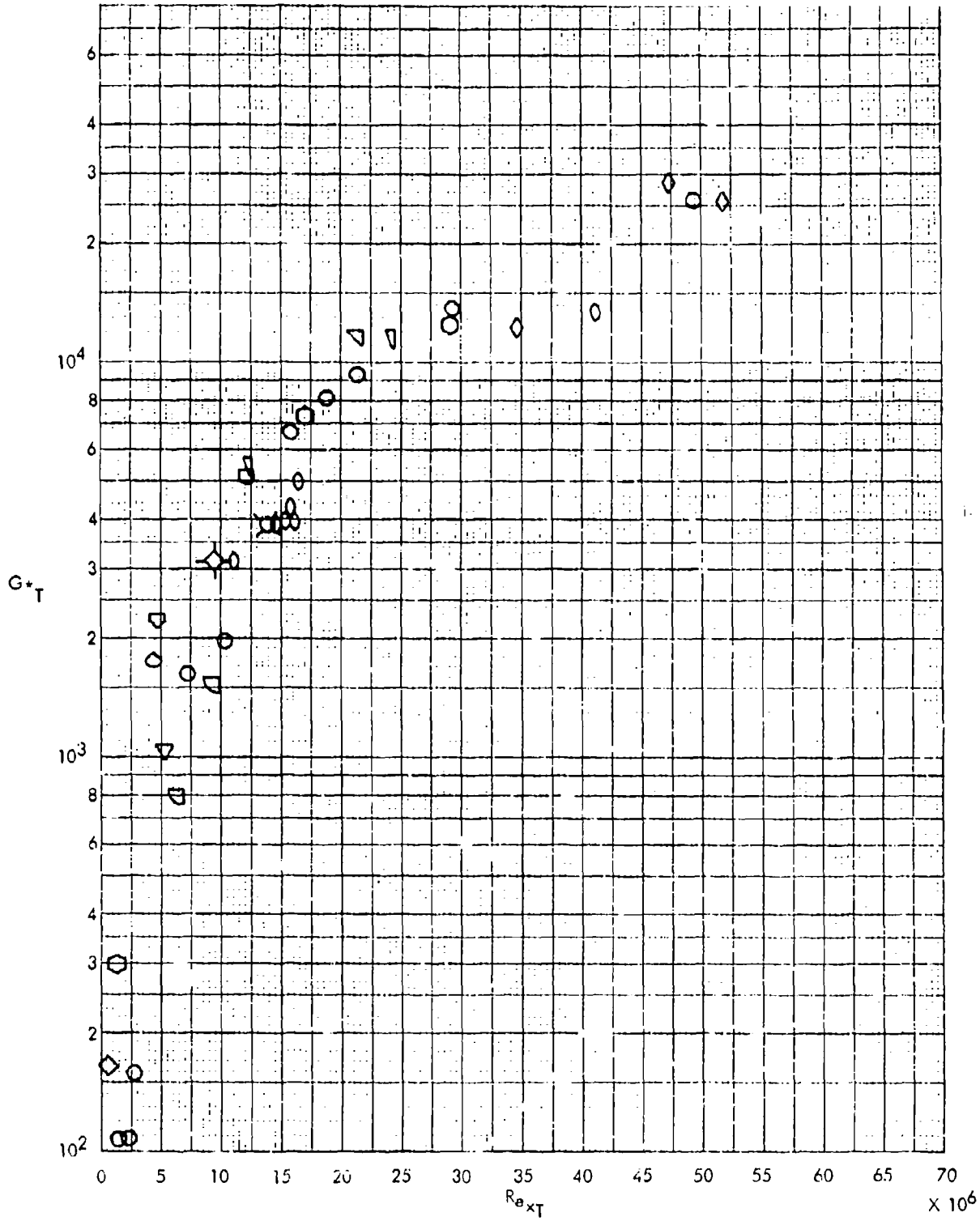

FIG. 2 (a) VARIATION OF TRANSITION PARAMETER G^*_T WITH TRANSITION REYNOLDS NUMBER Re_{xT} FOR FLIGHT DATA, EXPERIMENTAL DATA (See Table II)

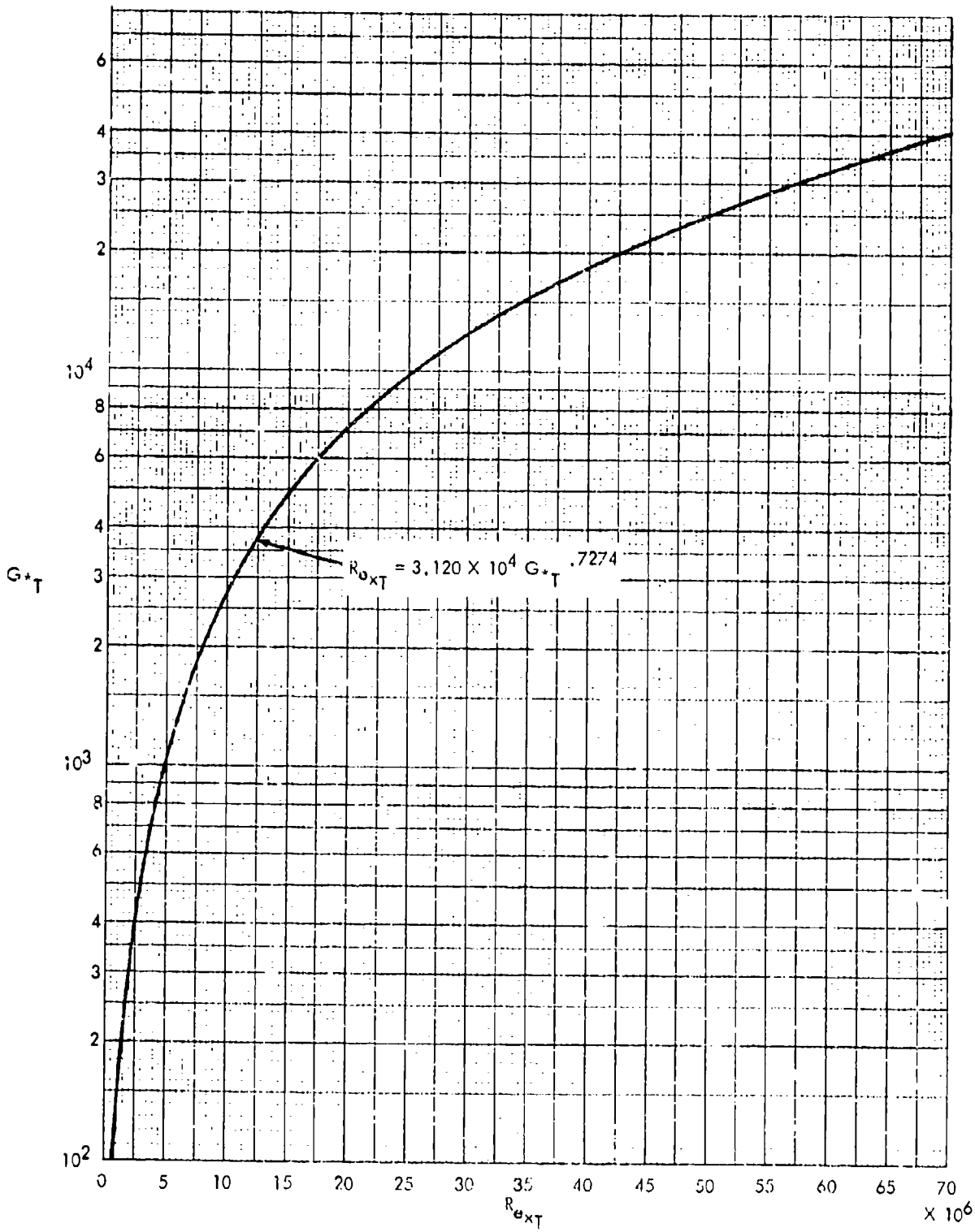

FIG. 2 (b) VARIATION OF TRANSITION PARAMETER G_{*_T} WITH TRANSITION REYNOLDS NUMBER $R_{\theta_{xT}}$ FOR FLIGHT DATA, LEAST SQUARES EQUATION FOR EXPERIMENTAL DATA.

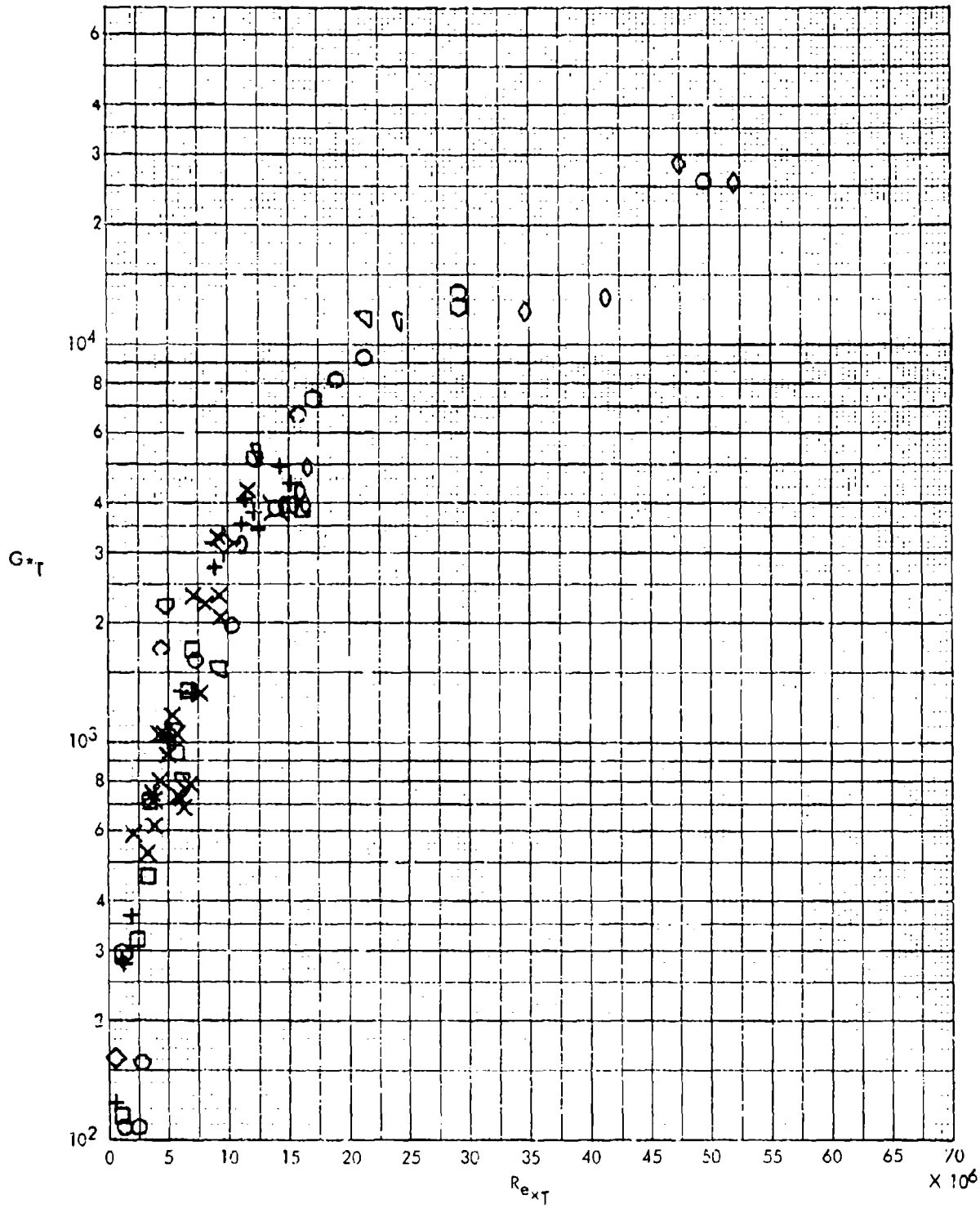

FIG. 3 (a) VARIATION OF TRANSITION PARAMETER G^*_T WITH TRANSITION REYNOLDS NUMBER $R_{e_{xT}}$ FOR BALLISTICS RANGE AND FLIGHT DATA, EXPERIMENTAL DATA.
(See Tables I and II)

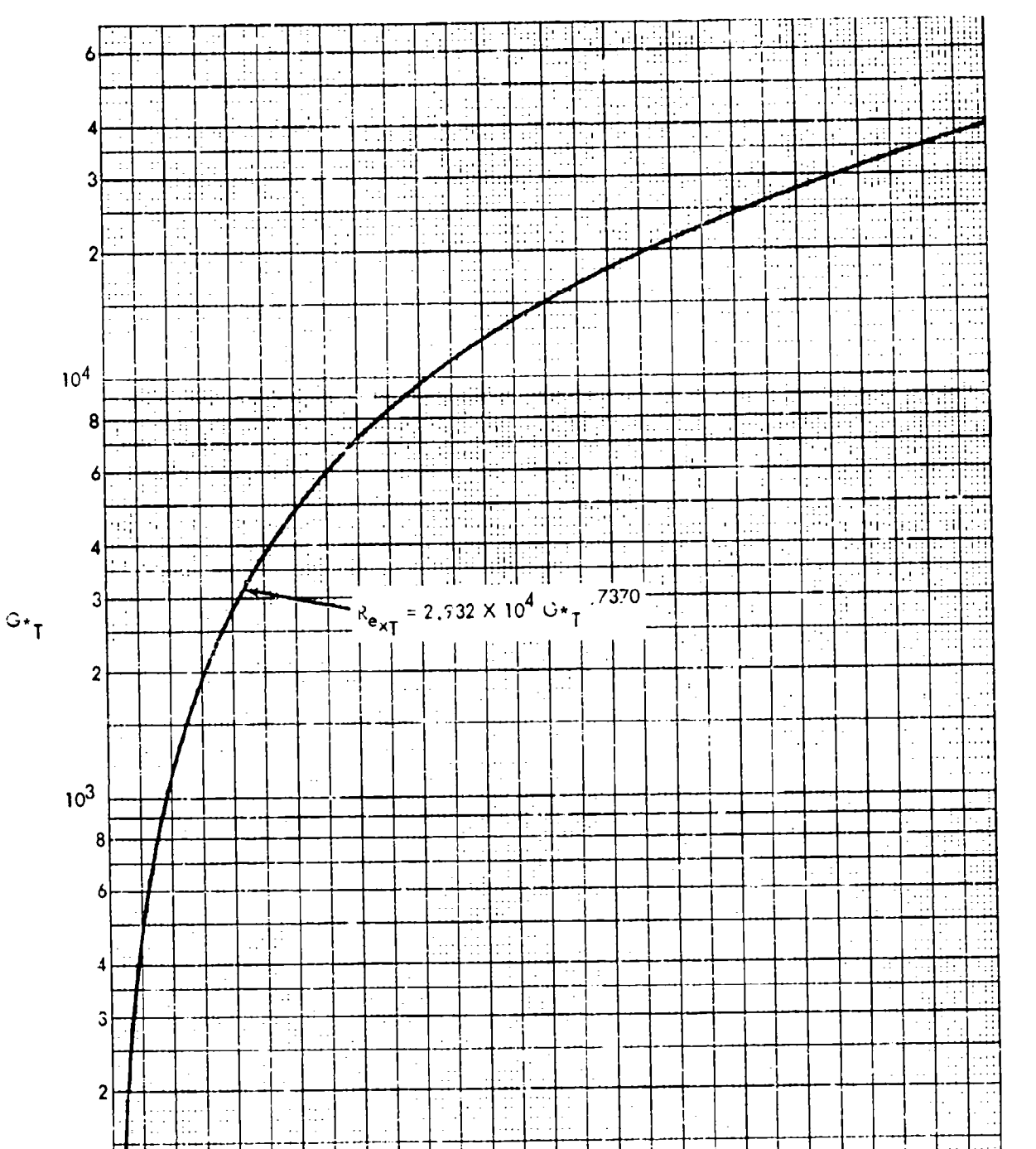

FIG. 3 (b) VARIATION OF TRANSITION PARAMETER G^*_T WITH TRANSITION REYNOLDS NUMBER $R_{e_{xT}}$ FOR BALLISTICS RANGE AND FLIGHT DATA, LEAST SQUARES EQUATION FOR EXPERIMENTAL DATA.